Kinetics of Microbubble–Solid Surface Interaction and Attachment

Chun Yang
School of Mechanical and Production Engineering, Nanyang Technological University, Singapore 639798

Tadeusz Dabros
CANMET Western Research Centre, Devon, AB T0C 1E0, Canada

Dongqing Li
Dept. of Mechanical and Industrial Engineering, University of Toronto, Toronto, ON M5S 3G8, Canada

Jan Czarnecki
Syncrude Canada Ltd., Edmonton Research Centre, Edmonton, Alberta T6N 1H4, Canada

Jacob H. Masliyah
Dept. of Chemical and Materials Engineering, University of Alberta, Edmonton, Alberta T6G 2G6, Canada

Microbubble–solid surface interaction and attachment under the influence of hydrodynamic and physicochemical forces were studied experimentally and theoretically. An impinging-jet technique was developed to measure bubble-attachment flux onto a flat solid surface in an impinging-jet stagnation flow. A video imaging system enables direct observation of the attachment behavior of hydrogen microbubbles onto two different collector surfaces: hydrophilic untreated glass and hydrophobic methylated glass. Experimental results showed that the attachment flux depends on both hydrodynamic flow and electrolyte concentration. A mass-transfer model developed computes bubble-attachment flux, considering hydrodynamic convection, Brownian diffusion, migration under gravitational buoyancy, and DLVO surface forces (that is, van der Waals and electric double-layer forces). At high flow rates, the numerical predictions for attachment rates onto methylated glass generally agreed well with the experimental data. However, a difference exists between theoretical and experimentally determined attachment rates for both untreated and methylated glass when the Reynolds number of the flow is low. Several mechanisms are proposed to account for this discrepancy.

Introduction

Attachment of microbubbles onto surfaces (referred to as collectors) is important to the success of many industrial and environmental separation processes, such as mineral extraction, bitumen recovery, and treatment of potable water and wastewater. From a theoretical perspective, the process of microbubble attachment can be conceptually divided into four stages: (1) at large distances from the collector, bubble transport in the bulk fluid is determined by convection and migration due to external forces such as buoyancy and fluid drag. (2) As a bubble approaches the collector within a distance comparable to the bubble size, displacement of the fluid between the bubble and the collector leads to additional hydrodynamic drag on the bubble. The resulting reduction in bubble mobility is referred to as the particle-wall hydrodynamic interaction (Kim and Karrila, 1991). (3) At even closer distances to the collector (1–100 nm), bubble motion is also affected by at least two types of well-recognized colloidal forces: first, the van der Waals (VDW) interaction becomes significant within such a range; second, due to the presence of electrostatic charges at the gas–solid–liquid interfaces, the elec-

Correspondence concerning this article should be addressed to J. H. Masliyah.

tric double-layer (EDL) interaction may develop within distances of the order of the Debye length from the collector (Hunter, 1981). These two colloidal interactions form the basis of the well-known Derjaguin–Landau–Verwey–Overbeek (DLVO) theory of colloidal stability. Further, other forces not accounted for by the DLVO theory, such as steric and hydrophobic interactions, may be important to bubble attachment under certain physicochemical conditions. In addition, stochastic effects originating from discrete surface charges and surface roughness could play a pronounced role at such separations (Czarnecki, 1984, 1986; Czarnecki and Dabros, 1980). Once a bubble is brought close to the collector surface within an immobilization distance that usually is in the same range as the so-called primary energy minimum (about a few nanometers), bubble attachment is considered to take place. (4) Beyond the immobilization distance, the bubble is considered in physical contact with the collector. This step involves many complex phenomena, some of which are difficult to define. It becomes clear that traditional continuum mechanics break down at such dimensions, and no theory is available to quantitatively describe the physical processes at such a stage (Anderson, 1989). Therefore, for simplicity, the present study focuses only on the transport of microbubbles from a flowing liquid to the immobilization distance.

Most of the existing theoretical analyses focus on the capture of non-Brownian, micrometer-sized particles by a single, large gas bubble (being of the order of millimeters in diameter). Different theories have been developed to predict the bubble–particle collision efficiency that is related to the particle capture rates. The simplest one, due to Smoluchowski, neglects the hydrodynamics of bubble–particle interaction and assumes that the bubble and the particle follow exactly straight trajectories. A slightly more advanced theory by Luttrell and Yoon (1992) assumes that the particles follow the streamlines of the rising bubble. Loewenberg and Davis (1994) presented a model for calculating the collision efficiency to include the hydrodynamics of the collision process as well as the VDW interactions. Recently, a more comprehensive model was developed by Leppinen (1999) to incorporate the exact hydrodynamics of bubble–particle interactions under the influence of both the VDW and EDL interactions.

The diffusion capture of Brownian particles has also been studied extensively. Acrivos and Taylor (1962) considered the capture of diffusing point particles by a rising sphere. Later, Prieve and Ruckenstein (1974) developed expressions for predicting the capture rates of spherical Brownian particles under hydrodynamic flow conditions. Recently, attempts were made to account for the VDW attraction, Brownian motion, and the EDL and hydrodynamic interactions (Ramirez et al., 1999).

Several experimental studies tackling bubble–particle interaction and attachment have been reported to investigate the effects of electrolyte concentration and pH (Fukui and Yuu, 1980), surface wettability (Vinke et al., 1991), and inertial hydrodynamic interaction (Dai et al., 1998). Since column flotation techniques were used exclusively in these studies, only bulk-averaged information regarding bubble–particle interactions is available, and the results represent the net effect of hydrodynamics and colloidal surface forces. Furthermore, the hydrodynamic conditions created in these column flotation experiments are difficult to control and reproduce. The underlying phenomena are often so complex that it is difficult to find a unique interpretation of the results in terms of a comprehensive physical framework.

To gain insight into the underlying mechanisms involved in bubble–solid surface interaction and attachment, it is helpful to analyze a related but simpler and better-defined system. The impinging-jet technique provides such a system. It was pioneered by one of the authors (Dabros and van de Ven, 1983a, 1987), who studied deposition of latex particles onto a glass surface. This technique has subsequently been used in many research laboratories for the study of particle deposition, and it can also be used as a probe to characterize polymer adsorption (Dijt et al., 1990), examine particle detachment (Varennes and van de Ven, 1987), and study deposition of oil emulsions (Sanders et al., 1995). Further, new measurement technologies have been incorporated to allow for the study of submicrometer colloidal particles (Bohmer et al., 1998).

This work presents results of a study of bubble attachment onto a solid surface under well-controlled conditions using a modified impinging-jet technique, allowing for assessment of the applicability of the existing theories on bubble attachment. The advantages of the impinging-jet technique are manifold: It allows us to directly observe the attachment process in the vicinity of the stagnation point where colloidal interactions are thought to play an important role and hydrodynamic conditions are well defined. From a physical viewpoint, the attachment of microbubbles onto a solid surface in the impinging jet is analogous to bubble–particle interaction and attachment occurring in a microflotation process. The flow pattern created around the stagnation point is very similar to that at the front end of a spherical collector (a solid particle) exposed to an induced uniform flow or settling due to gravity. Importantly, the quantitative nature of the short-ranged colloidal forces involved in the impinging-jet experiments is essentially the same as that acting during the flotation process of bubble–particle interaction and attachment. Although the importance of hydrodynamic and physicochemical effects is well recognized in the literature, there have been relatively few controlled studies of such effects on bubble attachment. Hence, one of the objectives of this work was to conduct a systematic study of microbubble attachment under various hydrodynamic flow intensities and solution ionic strengths. Another important goal was to generate experimental data that would enable the validation and improvement of bubble-attachment models.

Bubble-Attachment Experiments

Impinging jet system

The experimental apparatus is shown in Figure 1. In the test section, the impinging-jet cell is placed under a microscope. The cell itself consists of two parts connected by a glass capillary tube with an inner diameter (ID) of 2.65 mm. The upper part is used as an impingement chamber in which a glass slide (collector) is placed on the top to collect gas bubbles. The lower part serves as an electrolysis chamber. When an electrical potential is applied to the two electrodes, microsized hydrogen bubbles can be generated at the platinum wire (25 μm in diameter). Oxygen bubbles are produced on the counterelectrode that is separated from the

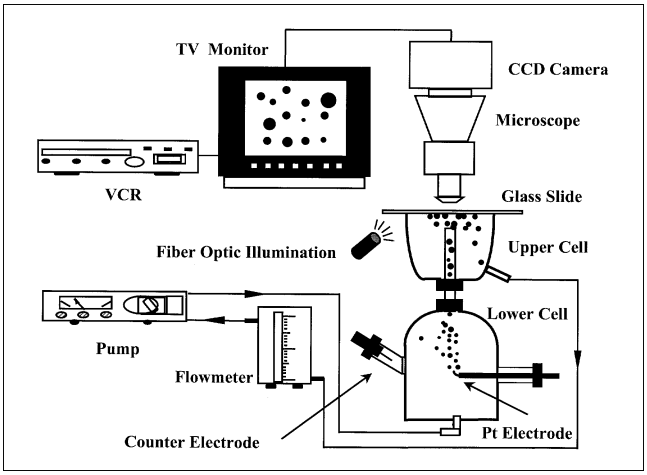

Figure 1. Experimental setup for performing the laboratory-scale bubble-attachment study.

lower cell (see Figure 1) by a microfilter to prevent possible contamination due to electrolytic reaction. The glass capillary has a length of $L = 50$ mm to ensure a sufficiently large ratio of L to ID, such that a fully developed flow is achieved at the tube exit. The distance between the capillary tube end and the collector was fixed at 2.65 mm during all experiments.

Electrolyte solution is introduced into the lower chamber from the bottom and carries hydrogen bubbles through the capillary tube. When the flowing jet exits at the tube outlet, it impinges on the glass collector. Bubbles that are not captured by the collector are swept away by the flow. The flow exits from the bottom corner of the upper cell and returns to the lower reservoir for circulation. The solution is then driven by a peristaltic pump to the upper reservoir to maintain a certain hydrostatic head so that a constant flow rate can be maintained. The flow rate is measured by a calibrated rotameter (Matheson, USA). The entire process of bubble attachment can be visually observed using a CCD camera and is recorded with a VCR for subsequent playback and analysis.

Experimental materials

Two types of model collector surfaces, untreated and methylated glass, were used to examine the effect of surface characteristics on bubble attachment. Precleaned microscope slides (Fisher Scientific) were chosen. The following cleaning procedure was used to prepare untreated glass collectors: the slides were first placed in an ultrasonic bath filled with deionized ultrafiltered (DIUF) water (Fisher Scientific) and 5% Ducan (a detergent for cleaning glassware) for 20 min, then rinsed thoroughly with DIUF water, and subsequently soaked in a mixing acid solution of three parts concentrated nitric acid to one part hydrochloric acid for 2 h. Afterwards, the slides were washed extensively with DIUF water and stored in DIUF water to protect the surface from contaminants. The methylated glass was prepared by immersing the untreated slides in a 20% v/v dimethyldichlorosilane (Aldrich) in toluene solution and soaked for about 4 h. The slides were then rinsed with methanol, dried in air, and stored in a glass jar. After treatment, a uniform, molecular hydrophobic film is formed on the glass surface due to chemical reaction (Araujo et al., 1995). Previous studies have shown that the film is very stable, even in aggressive chemical environments such as organic solvents.

Solutions were prepared using ACS-grade sodium chloride NaCl (BDH) dissolved in the DIUF water. At room temperature, the DIUF water has a conductivity of < 1.0 (μS/cm) and a surface tension (against air) of $\gamma_{wv} = 72.7 \pm 0.1$ (mN/m).

Experimental procedure

Because the stagnation-point region is susceptible to impurities, every attempt was made to maintain cleanliness of the system. All tubing was intensively washed and rinsed with DIUF water before use. Whenever the electrolyte solution was changed, a rigorous cleaning procedure, similar to that described for preparing untreated glass slides, was used to clean the impinging-jet cell, the glass capillary, and the two reservoirs. The entire loop was operated as a closed system to avoid possible contamination.

Experiments were carried out for a variety of hydrodynamic flow and aqueous solution conditions. During the experiment, the microscope was first adjusted in such a way that the stagnation point appeared at the center of the field of view, and the focus was on the bubbles attached on the collector. The attachment process was usually videotaped for 10–12 min. Through careful control of the current applied to the electrodes, the number of attached bubbles within the recording period was varied from 10 to over 100, depending on the experimental conditions. After bubble-attachment recording, the microscope focus was shifted to the outlet of the capillary tube to record the number of bubbles passing through the central circular section (100 μm in radius) of the tube exit for a given time interval (normally about 2–3 min). The total number of bubbles appearing in the field of view was in the range of 300–800 per min, and was directly related to the bulk bubble number concentration for a given flow rate. The attachment experiment was repeated at two locations for each glass slide, and two slides were used for each experimental condition. The final result was taken as the average of these four measurements. The recordings were used for the analysis of the bubble-attachment density and determination of bubble-size distributions and bubble bulk number concentrations.

Experimental Results

Characterization of glass collector surfaces

The characteristics of untreated and methylated glass slides were evaluated by contact angle measurements using the captive-bubble method by a goniometer (Rame-Hart Inc.). For each solution condition, five measurements were carried out by varying the air-bubble volume and changing the test location on the slides. Only receding contact angles were measured. Measurements were taken on both sides of each bubble and the readings were averaged. The results are summarized in Table 1. For untreated glass slides, bubble contact angle measurements could only be accomplished for bubbles that were immobilized on the slide surface. However, most of the freshly created bubbles slipped away very slowly, indicating a very small, perhaps zero, contact angle. Furthermore, it

Table 1. Measured Contact Angles for Untreated and Methylated Glass Collectors Using Captive Bubble Method

NaCl Aqueous Solution Molarity, M	pH Value	Contact Angle (°) (Untreated Glass)	Contact Angle (°) (Methylated Glass)
10^{-4}	7.0	7	102 ± 3
10^{-3}	7.0	12	104 ± 5
10^{-2}	7.0	10	99 ± 2
10^{-1}	7.0	7	100 ± 3

was observed that water droplets placed on the untreated glass slide spontaneously spread over the surface, demonstrating a high-energy, hydrophilic surface for such collectors. Nonetheless, average contact angles for the untreated glass were less than 10°. On the other hand, contact angles for methylated glass slides were found to be larger than 90°, indicating that the surface of the methylated glass is hydrophobic. Moreover, measurement results showed no apparent dependence of contact angle on the electrolyte concentration.

Bubble-attachment results

The bubble-attachment density β (m^{-2}) is introduced to characterize bubble attachment results, and it is defined as the ratio of the number of attached bubbles N_t to the area of the stagnation region, chosen as a circular area of radius $R_s = 300$ μm

$$\beta = \frac{N_t}{\pi R_s^2} \tag{1}$$

Clearly, for given hydrodynamic and physicochemical conditions, the value of β depends on bulk bubble number concentration n_∞ (m^{-3}), which is not known *a priori.* With consideration of fluid flow and buoyancy effects, an approach has been developed to determine the bubble number concentration, which can be expressed as

$$n_\infty = \frac{N(t)/\Delta t}{2Q\left(\frac{r_c}{R}\right)^2\left[1-\frac{1}{2}\left(\frac{r_c}{R}\right)^2\right] + \pi r_c^2 u_g}, \tag{2}$$

where $N(t)$ is the number of bubbles passing through the central region of the tube exit with radius; $r_c = 100$ μm over a given time Δt(s); Q is the volumetric flow rate of the solution measured during the experimental test; and R is the inner radius of the capillary tube. The rise velocity of the hydrogen gas in a stagnant liquid u_g is introduced to account for the buoyancy effect on the bubble, and its value is determined by Stokes' law. A detailed derivation of Eq. 2 is given elsewhere (Yang, 2000).

The normalized bubble-attachment density β^* is then defined as

$$\beta^* = \frac{\beta}{n_\infty}. \tag{3}$$

With β^* plotted against time t, the experimentally determined normalized bubble-attachment flux $j^*_{\exp}$, having the units of m/s, is obtained from the initial slope of the curve

$$j^*_{\exp} = \left.\frac{d\beta^*}{dt}\right|_{t=0} \tag{4}$$

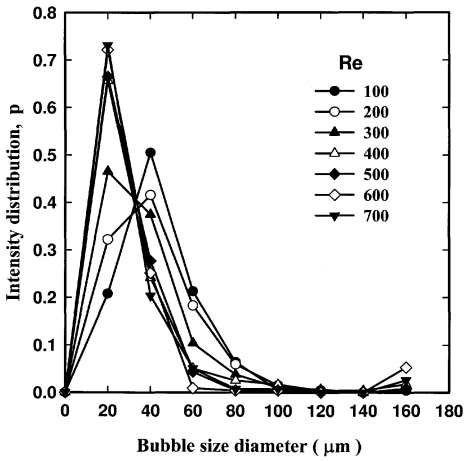

Figure 2. Bubble-size distributions at various Reynolds numbers (10^{-3} M NaCl at pH = 6.5).

Bubble size was analyzed from the same recording. By playing back the videotape at a slow speed, bubble size was estimated by randomly selecting a few hundred bubbles rolling on or approaching the glass slide. Figure 2 shows the bubble-size distributions measured in a 10^{-3}-M NaCl solution for various Reynolds numbers. For the impinging-jet system, the Reynolds number is defined as $Re = \rho_f V_o R/\mu_f$ (where V_o is the mean velocity at the capillary exit, and ρ_f and μ_f are the density and the dynamic viscosity of the solution, respectively). It can be observed that the diameter of most bubbles falls in the range from 10 μm to 80 μm, with an average size of 20–30 μm, consistent with the results reported by Burn et al. (1997). Furthermore, the bubble size is strongly dependent on the Reynolds number. In addition, as expected, observations showed that the number of bubbles produced per unit time is related to the electric current. However, it appears that the bubble-size distribution is not correlated with the solution concentration.

Bubble attachment is considered to take place when a bubble adheres on the glass slide. This criterion includes those bubbles that attach to the glass slide for a short duration and are then swept away by the flow. A typical bubble-attachment pattern is displayed in Figure 3. One can see that the attached bubbles were nearly evenly distributed in the field of view, suggesting that all the bubbles have the same probability of accessing the homogenous collector surface. In other words, the observation shows that the bubble-attachment flux is uniform over the viewing region near the stagnation point. This is an important feature of the impinging-jet technique and can be predicted from theory (Yang, 2000).

Figure 4 shows the normalized bubble-attachment density on methylated glass as a function of time under the Reynolds number varying from 100 to 700 in a 10^{-2}-M NaCl solution. As can be observed from Figure 4, the variation of the normalized bubble-attachment density with time is described very

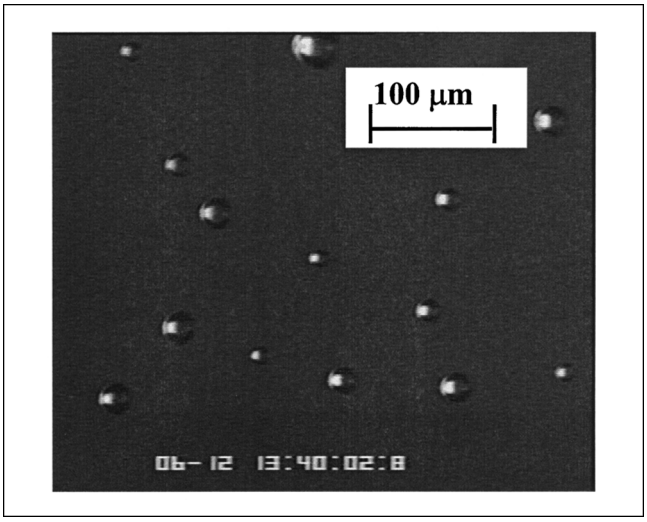

Figure 3. Bubble-attachment patterns on a collector surface.

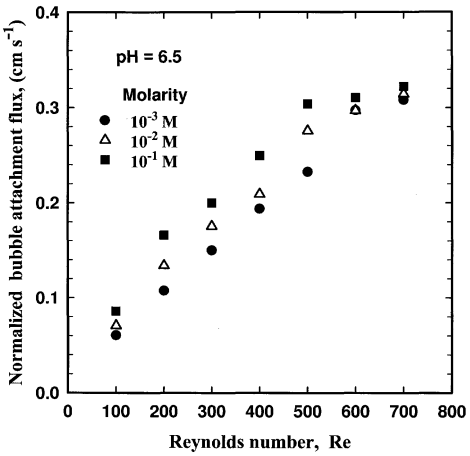

Figure 5. Variation of the normalized bubble-attachment flux to the methylated glass surface with the Reynolds number for different concentrations of the solution.

well by a linear function, confirming the absence of the so-called blocking effect. The blocking effect on particle deposition, giving rise to the nonlinearity of deposition rate with time due to masking effects by the already deposited particles, was discussed at length by Dabros and van de Ven (1982, 1983a,b). They demonstrated that the blocking effect is dependent, not only on the change of the collector surface topology and modification of local hydrodynamic conditions near the collector surface due to the deposited particles, but also on the alteration of the intrinsic colloidal interactions. The absence of the blocking effect in the present experiments could be attributed to the use of a sufficiently low bulk bubble concentration, as well as the fact that small bubbles (less than 40 μm) usually dissolved within a minute after attachment onto the glass slide. Furthermore, the observed linear behavior of the normalized bubble-attachment density also suggests a constant rate of bubble-attachment, ensuring that the obtained normalized bubble-attachment flux j^*_{exp} no longer represents the initial attachment flux as originally defined in Eq. 4. In fact, j^*_{exp} is a mean attachment flux over the *entire* experiment duration, and hence it represents a more reasonable measure of the bubble-attachment rate in the stagnation region.

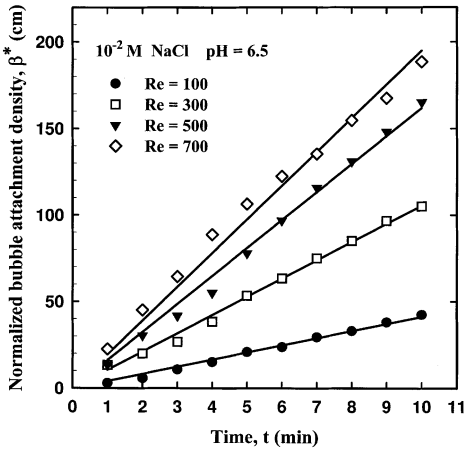

Figure 4. Experimental results for normalized bubble attachment density on the methylated glass vs. time for different Reynolds numbers, obtained while keeping both solution concentration and pH constant.

The solid lines were obtained from a least-squares linear regression.

Bubble attachment was investigated for NaCl solutions at three different molar concentrations: 10^{-3} M, 10^{-2} M, and 10^{-1} M, and the results for the normalized bubble-attachment flux onto the methylated glass are given in Figure 5. This figure amply shows that bubble attachment is noticeably affected by the electrolyte concentration, as well as the hydrodynamic flow conditions. Larger values of bubble-attachment flux were observed at higher electrolyte concentrations and *Re* numbers. The derivation of a theoretical model to rationalize the experimental results just noted follows below.

Theoretical Model

Consider a dilute suspension of spherical, noninteracting microbubbles dispersed in a flowing jet characterized by the fluid velocity vector v. Under steady-state conditions, the mass conservation equation governing the bubble-attachment process takes the form

$$\nabla \cdot j = 0 \tag{5}$$

The bubble flux j accounting for contributions due to convection, diffusion, and migration under colloidal and external force fields is expressed by (van de Ven, 1989; Masliyah, 1994)

$$j = un - \underline{D} \cdot \nabla n + \underline{D} \cdot F \frac{n}{kT} \tag{6}$$

where u is the bubble velocity, n is the local number concentration of bubbles, $\underline{D}$ is the bubble-diffusion coefficient ten-

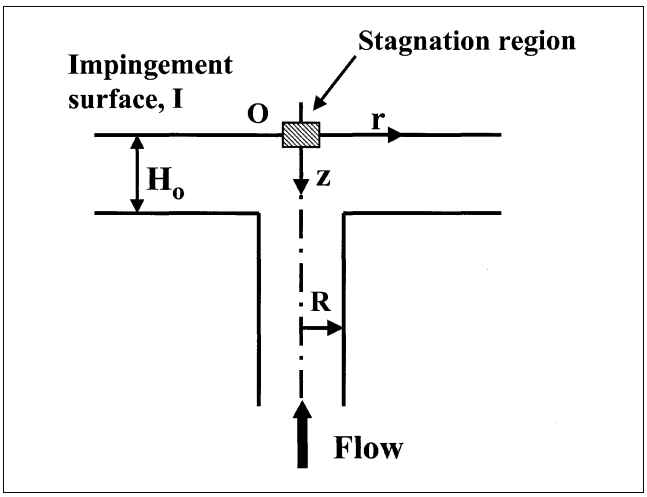

Figure 6. Geometry of the impinging jet cell.

A liquid jet enters a capillary tube of radius R and then impinges onto a collector surface I with a separation distance of H_o. The stagnation point O, located on the axis of symmetry and the impingement surface I, is the origin of the cylindrical coordinate system r and z.

sor, k is the Boltzmann constant, T is the absolute temperature, and $\boldsymbol{F}$ is the total force acting on a bubble. To solve the flux conservation equation (Eqs. 5 and 6), one needs to know the bubble velocity, the bubble diffusion coefficient, and all the forces acting on a bubble.

Fluid flow field and bubble velocity

Figure 6 illustrates the geometric configuration of the impinging-jet flow. As the fluid flow is axisymmetric, the flow field can be best described using a two-dimensional cylindrical coordinate system, with the origin located at the stagnation point O. Since the bubble concentration in the flow stream is dilute (the volume fraction is less than 1%) in our experiments, the effect of the presence of the bubbles on the flow field can be neglected. With the assumption of Newtonian, incompressible, laminar flow under steady-state conditions, the flow field is governed by the Navier–Stokes equations. No-slip boundary conditions are applied to the solid walls and a parabolic velocity profile is assumed at the capillary exit. The numerical approach used to solve the Navier–Stokes equations essentially follows Deshpande and Vaishnav (1982), and a detailed description can be found elsewhere (Yang, 2000).

With respect to bubble attachment, the region of interest is near the stagnation point where the colloidal surface forces between a bubble and the collector surface are thought to play an important role. With this in mind, the flow velocities near the stagnation point are approximated by

$$\bar{v}_r = \bar{\alpha}\bar{z}\bar{r} \qquad \bar{v}_z = -\bar{\alpha}\bar{z}^2 \tag{7}$$

where

$$\bar{r} = \frac{r}{R} \qquad \bar{z} = \frac{z}{R} \qquad \bar{v}_r = \frac{v_r}{V_o} \qquad \text{and} \qquad \bar{v}_z = \frac{v_z}{V_o}.$$

Here v_r and v_z are the fluid velocity components along the r and z coordinates, respectively. The dimensionless parameter $\bar{\alpha}$ characterizes the intensity of the flow. For a fixed separation $\bar{H}_o = 2$, values of $\bar{\alpha}$ for different Reynolds numbers were obtained by fitting Eq. 7 to the numerical results of the Navier–Stokes equations for the flow velocity distributions. Correlation of $\bar{\alpha}$ vs. Re obtained by performing regression analysis is given by

$$\bar{\alpha} = 5.3\ Re^{0.5} - 8.13 \qquad (Re \geq 5) \tag{8}$$

In order to evaluate the valid range where stagnation point flow patterns can be used to describe the fluid flow in the impingement region, a series of numerical tests was performed for various Re values. The results show that Eqs. 7 and 8 can be used to characterize the flow field around the stagnation point for $\bar{r} \leq 0.25$ and $\bar{z} \leq 0.1$, corresponding to $r = 330\ \mu$m and $z = 130\ \mu$m when the radius of the capillary tube used in the experiments is $R = 1.325$ mm.

The bubble velocity, $\boldsymbol{u}$, induced by the fluid motion is, in general, different from the undisturbed fluid velocity $\boldsymbol{v}$, because of the bubble–wall hydrodynamic interaction. The relationships between $\boldsymbol{u}$ and $\boldsymbol{v}$ near the collector surface are given by

$$u_r = v_r f_3(z) \qquad u_z = v_z f_1(z) f_2(z) \tag{9}$$

Here, z is the distance from the center of the bubble to the collector surface, $f_1(z)$, $f_2(z)$, and $f_3(z)$ are universal hydrodynamic functions accounting for the deviations from the Stokes drag.

Bubble diffusion coefficient (diffusivity)

Near the collector, the diffusion coefficient becomes dependent on the relative positions and orientations of the bubble and the wall (that is, it becomes a tensor quantity), and the bubble diffusion-coefficient components are formulated as (van de Ven, 1989; Masliyah, 1994)

$$\underline{\boldsymbol{D}} = \begin{pmatrix} D_{rr} & D_{rz} \\ D_{zr} & D_{zz} \end{pmatrix} = D_\infty \begin{pmatrix} d_{rr} & 0 \\ 0 & d_{zz} \end{pmatrix} = D_\infty \begin{pmatrix} f_4(z) & 0 \\ 0 & f_1(z) \end{pmatrix} \tag{10}$$

where D_∞ is the bubble Brownian diffusion coefficient in the bulk unbounded phase, and is determined from the Stokes–Einstein equation

$$D_\infty = \frac{kT}{6\pi\mu_f a_p} \tag{11}$$

Here a_p is the radius of the gas (hydrogen) bubble. Rigorous derivations of $f_1(z)$, $f_2(z)$, $f_3(z)$, and $f_4(z)$ are well documented in the literature by Goldman et al. (1967) and Goren and O'Neill (1971).

Forces acting on a bubble

The total forces acting on a microbubble are assumed to consist of the gravitational buoyant force and DLVO surface

forces (that is, the VDW and EDL interaction forces).

$$\boldsymbol{F} = \boldsymbol{F}_{Gr} + \boldsymbol{F}_{VDW} + \boldsymbol{F}_{EDL} \tag{12}$$

The net gravitational force, nondimensionlized with respect to the Brownian kinetic energy over bubble radius (kT/a_p), is expressed as

$$\bar{F}_{Gr} = \frac{4\pi}{3}\frac{\Delta\rho g a_p^4}{kT} \tag{13}$$

where $\Delta\rho = \rho_p - \rho_f$ is the density difference between the bubble ρ_p and the aqueous solution ρ_f. In the impinging-jet setup shown in Figure 1, bubbles are transported upward to the collector, indicating that the net gravitational force acts favorably to the attachment process.

The dimensionless VDW interaction force between a sphere and a flat plate, with consideration of the retardation effect, is approximately formulated as (Suzuki et al., 1969)

$$\bar{F}_{VDW} = \frac{F_{VDW}}{\left[\frac{kT}{a_p}\right]} = -Ad\frac{\bar{\lambda}}{\bar{h}^2}\frac{(\bar{\lambda} + 22.232\bar{h})}{(\bar{\lambda} + 11.116\bar{h})^2} \tag{14}$$

where

$$Ad = \frac{A_{132}}{6kT} \qquad \bar{\lambda} = \frac{\lambda}{a_p} \qquad \text{and} \qquad \bar{h} = \frac{h}{a_p} = \frac{z - a_p}{a_p}$$

Here Ad is referred to as the adhesion number, and it is a measure of the strength of the VDW interaction; A_{132} is the Hamaker constant for the VDW interaction between phase 1 (bubble) and phase 2 (glass collector) separated by a liquid medium, phase 3; λ is the retardation wavelength, usually taken as 10^{-7} m; and h is the separation gap between the bubble and the collector. Following Israelachvili (1985), A_{132} for a gas–water–solid system is given by

$$A_{132} \approx \left(\sqrt{A_{11}} - \sqrt{A_{33}}\right)\left(\sqrt{A_{22}} - \sqrt{A_{33}}\right) \tag{15}$$

Usually, the effective Hamaker constant A_{132}, for a gas–water–solid system is negative, suggesting that the VDW interaction in this situation is repulsive in nature. Published values for the Hamaker constant for gas, glass, and water are $A_{11} = 4.1\times10^{-26}$ J, $A_{22} = 14.7\times10^{-20}$ J, and $A_{33} = 4.38\times10^{-20}$ J, respectively (Vincent, 1973). Accordingly, the Hamaker constant and the adhesion number for the gas–water–untreated glass system are, respectively, calculated as $A_{\text{untreated}} = -3.64\times10^{-20}$ J and $Ad = -1.2$. The Hamaker constant of the gas–water–methylated glass system, however, requires additional attention because a thin film was formed during the glass surface treatment process. The presence of such a thin film not only modifies the hydrophobicity of the glass surface, as demonstrated in the contact-angle measurements, but also affects the VDW interaction between a bubble and the glass collector. The effect of a thin layer on the VDW interaction was discussed by Usui and Barouch (1990). The effective Hamaker constant for the methylated glass–water–spherical gas bubble at a separation distance h from a flat glass plate, as shown in Figure 7, can be expressed as

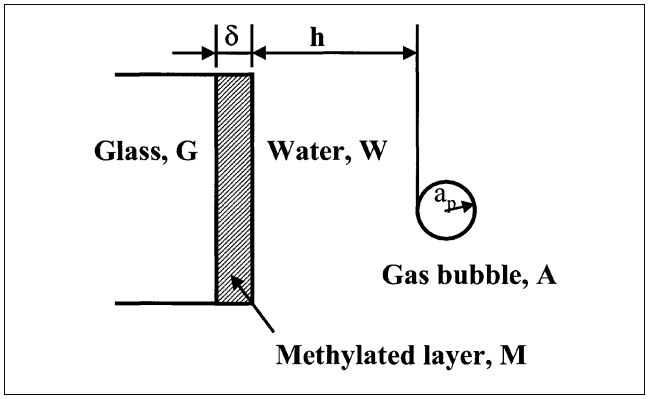

Figure 7. van der Waals interaction for the methylated glass–water–gas bubble system.

$$A_{132} = \left(\frac{a_p + \delta}{a_p}A_a + \frac{h}{h+\delta}A_b + \frac{a_p+\delta}{a_p}A_c + \frac{h}{h+\delta}A_d\right) \tag{16}$$

$$A_a = \left(\sqrt{A_{mm}} - \sqrt{A_{33}}\right)\left(-\sqrt{A_{33}}\right)$$

$$A_b = \left(\sqrt{A_{22}} - \sqrt{A_{mm}}\right)\left(-\sqrt{A_{33}}\right) \tag{17a}$$

$$A_c = \left(\sqrt{A_{mm}} - \sqrt{A_{33}}\right)\left(\sqrt{A_{11}}\right)$$

$$A_d = \left(\sqrt{A_{22}} - \sqrt{A_{mm}}\right)\left(\sqrt{A_{11}}\right). \tag{17b}$$

Here A_{mm} is the Hamaker constant of dimethyldichlorosilane under vacuum. With the methylated layer thickness δ being of order 10^{-9}, while the bubble radius a_p is of order 10^{-6} m, one can approximate $(a_p + \delta)/a_p \approx 1$. It is noted that the Hamaker constant for dimethyldichlorosilane is not available in the literature. However, the Hamaker constant for polymethylchlorine can be a good substitute; hence, we have $A_{mm} \approx 6.1\times10^{-20}$ J. Figure 8 gives the effective Hamaker constant for gas–water–methylated glass system, as calculated from Eq. 16 for various methylated layer thicknesses. As shown in Figure 8, compared with the Hamaker constant of the gas–water–untreated glass system, the negative Hamaker constant of the gas–water–methylated glass system is greatly reduced due to the effect of the methylated layer. Such an effect was included in the numerical calculations, in which the thickness of the methylated layer was chosen as 0.5 nm.

The frequently used simple HHF formula, due to Hogg et al. (1966), for quantitatively describing the EDL interaction force between a sphere and a flat plate, is expressed as

$$\bar{F}_{EDL} = \frac{F_{EDL}}{kT/a_p} = Dl\tau\left[\frac{\exp(-\tau\bar{h})}{1+\exp(-\tau\bar{h})} - Da\frac{\exp(-2\tau\bar{h})}{1-\exp(-2\tau\bar{h})}\right] \tag{18}$$

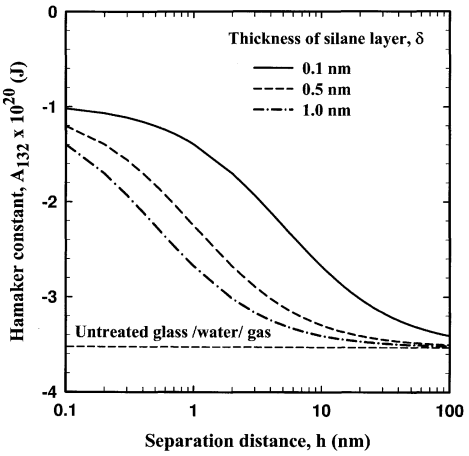

Figure 8. Calculated effective Hamaker constant for the methylated glass–water–gas bubble system.

The dimensionless groups are defined as

$$Dl = \frac{4\pi\epsilon_o\epsilon_r a_p \zeta_c \zeta_p}{kT} \qquad \tau = \kappa a_p \qquad Da = \frac{(\zeta_c - \zeta_p)^2}{2\zeta_c\zeta_p} \quad (19)$$

Here, ϵ_o is the permittivity of vacuum and ϵ_e is the dielectric constant of the solution; ζ_p and ζ_c are the zeta potentials of the bubble and the collector, respectively; Dl is the double-layer parameter characterizing the strength of the EDL interaction; Da is the double-layer asymmetry parameter representing the portion of the EDL interaction arising from the difference between the zeta potentials of the bubble and the collector; τ is the dimensionless ionic strength; and the Debye–Hückel parameter κ is defined as

$$\kappa = \left(\frac{e^2 \Sigma n_{io} z_i^2}{\epsilon_o \epsilon_r kT}\right)^{1/2}$$

(e is the elementary charge, n_{io} is the bulk number concentration of type-i ions, and z_i is the valence of type-i ions).

Bubble transport equation

So far the bubble velocity, the bubble diffusion coefficient, and the total forces acting on a bubble are defined. If we assume zero radial components for the colloidal and external forces and neglect radial diffusion of bubbles in the stagnation point region, that is, $F_r = 0$ and $\partial n/\partial r = 0$, the bubble flux, defined in Eq. 6, can be expressed in dimensionless form as

$$\bar{j}_r = \frac{1}{2} f_3 Pe \bar{n} \bar{r} \bar{z} \quad (20a)$$

$$\bar{j}_z = -\frac{1}{2} f_1 f_2 Pe \bar{n} \bar{z}^2 - f_1 \frac{d\bar{n}}{d\bar{z}} + f_1 \bar{F}_z \bar{n}, \quad (20b)$$

where

$$\bar{j}_i = \frac{a_p j_i}{D_\infty n_\infty} \quad (i = r, z), \qquad \bar{r} = \frac{r}{a_p}, \qquad \bar{z} = \frac{z}{a_p},$$

$$Pe = \frac{2\alpha a_p^3}{D_\infty}, \qquad \alpha = \bar{\alpha}\frac{\mu_f Re}{\rho_f R^3}, \qquad \bar{F}_z = \frac{F_z}{\left[\frac{kT}{a_p}\right]},$$

$$\bar{n} = \frac{n}{n_\infty}$$

With all forces acting on a bubble being defined in Eqs. 13, 14, and 18, the net axial force $\bar{F}_z$ can be explicitly formulated as

$$\bar{F}_z = \bar{F}_G + F_{VDW} + \bar{F}_{EDL}$$

$$= -Gr - Ad\frac{\bar{\lambda}(\bar{\lambda} + 22.232\bar{h})}{\bar{h}^2(\bar{\lambda} + 11.116\bar{h})^2}$$

$$+ Dl\tau\left[\frac{\exp(-\tau\bar{h})}{1+\exp(-\tau\bar{h})} - Da\frac{\exp(-2\tau\bar{h})}{1-\exp(-2\tau\bar{h})}\right] \quad (21)$$

Making use of Eqs. 20a and 20b, the flux conservation equation (Eq. 5) becomes

$$(1+\bar{h})Pef_3(\bar{h})\bar{n} = \frac{d}{d\bar{h}}\left\{f_1(\bar{h})\left[\frac{d\bar{n}}{d\bar{h}} + \frac{1}{2}(1+\bar{h})^2 Pef_2(\bar{h})\bar{n} - \bar{F}_z(\bar{h})\bar{n}\right]\right\} \quad (22)$$

which is subject to the following boundary conditions

$$\bar{n} = 1 \quad \text{as} \quad \bar{h} \to \infty \quad \bar{n} = 0 \quad \text{at} \quad \bar{h}_o = \bar{\gamma} = \frac{\gamma}{a_p} \quad (23)$$

The second boundary condition, referred to as a "perfect sink" approximation, has been used extensively to model particle deposition (Prieve and Ruckenstein, 1974; Adamczyk et al., 1983; Elimelech, 1991). The hypothetical situation described by this condition states that all particles are irreversibly captured by the collector surface once they reach a certain separation distance $\bar{\gamma}$, which is usually taken as the location of the primary energy minimum (PEM). In analogy to particle deposition analysis, bubble attachment is considered to occur when a bubble arrives at such an immobilization distance $\bar{\gamma}$. In the calculation, the value of $\bar{\gamma}$ was chosen as 5×10^{-4}. For a bubble of radius 5–20 μm, it corresponds to an absolute interception distance of 2.5–10 nm. Such a distance range exactly falls in the same order of magnitude of the primary minimum. Though the calculated attachment results are dependent on the choice of $\bar{\gamma}$, our calculation shows that the dependence is not strong if $\bar{\gamma}$ is chosen no less than 3×10^{-4}.

In principle, the transport equation (Eq. 22) is quite general, and is applicable to the deposition of spherical colloidal particles (such as solid particles, oil droplets) onto a solid surface in the impinging jet stagnation region. To make Eq. 22 applicable to microbubbles in the present analysis, the following additional conditions must be satisfied: (1) the bubble has to retain a spherical shape; (2) the hydrodynamic boundary layer should be thicker than the bubble diffusion boundary layer; (3) Stokes' law can be applied to the microbubble motion; and (4) the immobilization distance $\bar{\gamma}$ chosen should be smaller than the critical rupture thickness of the thin liquid film. It has been demonstrated by Yang et al. (1999) that all these conditions are fulfilled for microbubbles in the impinging-jet stagnation flow regime.

Bubble Attachment: Comparison of Experiments and Theoretical Predictions

After numerically solving the bubble transport equation (Eq. 22), one can obtain the theoretical values for the normalized bubble-attachment flux j_o^* which is expressed as

$$j_o^* = -\frac{f_1(\bar{\gamma})D_\infty}{a_p}\left(\frac{d\bar{n}}{d\bar{h}}\right)_{\bar{\gamma}} \tag{24}$$

Here j_o^* is the counterpart of the experimental normalized bubble attachment j_{exp}. In reality, bubbles generated in the impinging-jet experiments exhibit a wide range of sizes. To account for the bubble-size distribution, a mean bubble-attachment flux J_o^* can be calculated using the formula

$$J_o^* = \Sigma j_o^*(a_{pi})p(a_{pi}) \tag{25}$$

where $j_o^*(a_{pi})$ is the normalized bubble-attachment flux calculated on the basis of a uniform bubble size a_{pi}; and $p(a_{pi})$ is the bubble-size distribution intensity function with respect to a_{pi}, determined from bubble-size measurements, as shown in Figure 2. The mean flux J^*_o is then compared to the experimentally determined normalized bubble-attachment flux j^*_{exp} defined by Eq. 4.

The zeta potentials of the bubbles and the collector are needed to calculate the EDL interaction defined in Eq. 18. The zeta potential values for the glass collector surfaces were taken directly from the literature, and are listed in Table 2. However, the zeta potential of gas bubbles is not available, and a microelectrophoresis-type apparatus was developed for its measurement. Details of the experimental setup are provided elsewhere (Yang et al., 2001). The bubble zeta potentials are also provided in Table 2.

A comparison between the measured and calculated normalized bubble-attachment fluxes onto methylated glass surfaces for 10^{-2} M NaCl electrolyte is presented in Figure 9. Overall, as Figure 9 illustrates, the theoretical bubble-attachment flux to the methylated glass is in reasonable agreement with the experimental results, suggesting that the process of microbubble attachment onto the methylated glass can be satisfactorily described by the bubble transport equation developed on the basis of the DLVO theory. However, the experimental data for the low range of Reynolds numbers ($100 \le Re \le 300$) gave bubble-attachment fluxes that are higher than the theoretical predictions. The discrepancy in the attachment flux values is likely caused by other factors such as stochastic contributions that are not included in the present model development. A brief discussion of these factors and, particularly, their possible influence on bubble-attachment flux will be presented.

Table 2. Zeta Potentials of Hydrogen Gas Bubbles and Glass Collectors

NaCl Aqueous Solution Molarity, M	ζ_b (mV)* Bubbles	ζ_c (mV)** Methylated Glass	ζ_c (mV)† Untreated Glass	Remarks
10^{-4}	−50	−48	−82	
10^{-3}	−38	−35	−71	
10^{-2}	−27	−23	−63	pH = 6.5–7.0
10^{-1}	−18	−11	−30	

*Hydrogen gas bubble zeta-potential data are measured in this work.
**Methylated glass zeta-potential data are quoted from references.
†Untreated glass zeta-potential data are quoted from references.

The effect of the electrolyte concentration on the normalized bubble-attachment flux is presented in Figure 10. This figure shows that the measured attachment flux monotonically increases as the concentration of NaCl increases from 10^{-4}M to 10^{-1} M, while keeping the same conditions of $Re = 200$ and pH = 6.5. The theoretical attachment flux curve follows the same trend as the experimental results over the range of electrolyte concentrations under study. Although there is a difference between the theoretical predictions and experimental measurements, the proposed model captures the basic features of bubble-attachment. The increase in the bubble attachment flux with electrolyte concentration can be understood as follows: as the electrolyte concentration increases from 10^{-4} M to 10^{-1} M, the reciprocal of the Debye–Hückel parameter κ^{-1} decreases from 32 nm to 1 nm. Also, as shown in Table 2, the corresponding zeta potentials

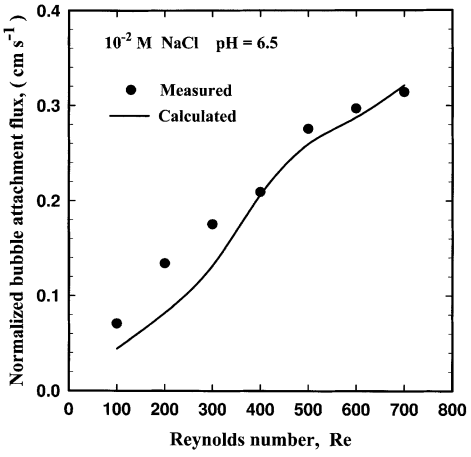

Figure 9. Variation of the normalized bubble-attachment flux to the methylated glass surface with the Reynolds number for fixed solution concentration and pH values.

Symbols represent experimentally measured flux j^*_{exp}, defined by Eq. 4; solid line is the calculated mean attachment flux with bubble-size distribution correction J_o^*, defined by Eq. 25.

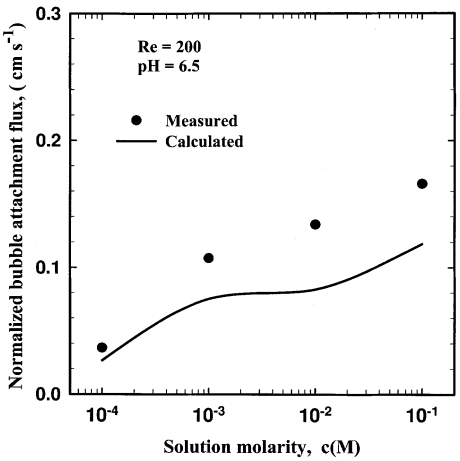

Figure 10. Variation of the normalized bubble-attachment flux to the methylated glass surface with NaCl solution concentration under a fixed Reynolds number *Re* = 200.

Symbols represent experimentally measured flux j^*_{exp}, defined by Eq. 4; solid line is the calculated mean attachment flux with bubble-size distribution correction J^*_o, defined by Eq. 25.

of the bubbles and the methylated glass decrease from −50 mV and −46 mV to −18 mV and −11 mV, respectively. As a result, the repulsive EDL interaction is greatly reduced at higher salt concentrations, leading to higher bubble attachment rates.

Figure 11 summarizes the results of experiments for bubble attachment onto the untreated glass surface carried out with 10^{-2} M NaCl. The corresponding calculated attachment flux is included for comparison. It is observed that when the Reynolds number is high, as when $Re \geq 400$, the proposed model provides a fairly good prediction for bubble attachment onto the untreated glass surface. However, the theoretical model fails to predict bubble attachment onto the untreated glass for the low-range Reynolds numbers (that is, $100 \leq Re \leq 300$).

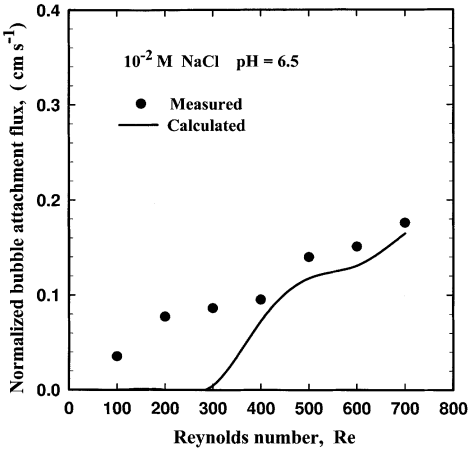

Figure 11. Variation of the normalized bubble attachment flux to the untreated glass surface with the Reynolds number for given solution concentration and pH values.

Symbols represent experimentally measured flux j^*_{exp}, defined by Eq. 4; solid line is the calculated mean attachment flux with bubble size distribution correction J^*_o, defined by Eq. 25.

Deviation of Theory from Experiment at Low Reynolds Numbers

Although it has been shown that the theoretical predictions agree well with the experimental results at Reynolds numbers of $400 \leq Re \leq 700$, theoretical predictions deviated from experimental data for both untreated and methylated glass surfaces for Reynolds numbers between $100 \leq Re \leq 300$. In particular, for the untreated glass, the theoretical predictions that bubbles would not attach to the glass surface until *Re* reaches 300, above which a drastic increase in bubble-attachment flux would occur, was not observed in the experiments. The experimental data, however, showed a gradual and continuous increase in attachment as the hydrodynamic conditions become increasingly favorable to the attachment process where *Re* increases from 100 to 700. It should be noted that, despite experimental evidence, the scenario of gas-bubble attachment onto untreated glass is difficult to explain using the existing classic thin-film theory (Sharma and Jameel, 1993). According to the literature, the prerequisite condition for bubble attachment onto a solid surface is that thin-film rupture must occur. Film rupture is associated with the instability of the thin film, which, in turn, is determined by the colloidal interactions between the bubble and the collector surface. Since the present situation involves the interaction of a hydrophobic gas bubble and hydrophilic untreated glass in a 10^{-2}-M NaCl solution, there are clearly no short-range attractive forces, such as hydrophobic or hydration forces. As addressed earlier, both VDW and EDL interactions are repulsive for the bubble–water–glass system. Overall, bubble attachment onto the untreated glass can be considered to occur under unfavorable conditions. Then, two questions arise: What is the driving force for the bubbles to attach onto the untreated glass surface? Why is there a discrepancy between theory and experiment? It has frequently been reported in the literature that when the deposition conditions are unfavorable, measured rates of particle deposition are found to be orders of magnitude greater than predicted values (Czarnecki, 1986; Elimelech and O'Melia, 1990; Walz, 1998). As yet, it is not clear what are the real sources for such discrepancies. It has been recognized that rigorous application of the DLVO theory is restricted to a model system under thermodynamic equilibrium. Assumptions employed in the theory are that the two interacting surfaces, a bubble and the collector, are ideally smooth and homogenous and have deterministic values of surface properties (such as the zeta potential). In reality, any test surface is, to some degree, rough and heterogeneous. Considering this fact, several hypotheses have been proposed to explain the observed bubble attachment onto glass surfaces; these are asymmetric EDL interaction, effect of adsorbed layer on the VDW interaction, presence of nanobubbles on collector surfaces, heterogeneity of surface charge density and roughness, and dynamic nature of the EDL.

The hypothesis of asymmetric EDL interaction implies the existence of a short-range (less than the Debye length) attrac-

tive interaction between two charged interfaces having the same sign but different surface potentials (Yang et al., 1999). This short-range attractive interaction can always be predicted within the framework of a constant potential using the Poisson–Boltzmann equation (McCormack et al., 1995). Recently, attraction force was observed between a pair of similarly charged colloidal spheres near a charged glass wall (Larsen and Grier, 1997). Despite experimental evidence, such observations are difficult to rationalize on the basis of existing theories. Yang et al. (1999) examined the role of the asymmetric EDL interaction in bubble attachment and demonstrated that, under certain circumstances, gas bubbles can attach onto a hydrophilic surface. However, under the experimental conditions of the present work, the reported data for the zeta potentials of the bubble and the untreated glass surface, respectively, are -27 mV and -23 mV (see Table 2), giving an asymmetric EDL interaction parameter of $Da = 0.013$. The value for Da is relatively small, and, hence the influence of asymmetric EDL interaction seems insufficient to result in a short-range attraction.

Another possible explanation could be that the bubbles usually contain surface-active impurities; this is difficult to avoid in the impinging-jet experiment. According to Usui and Barouch (1990), the presence of such an absorbed layer on bubbles could affect the VDW interaction at short distances. Their calculations showed that when a bubble is close to glass in water and is surrounded by a layer of surface-active molecules, the short-range VDW interaction is dominated by the effective Hamaker constant, which is positive. Thus, the possibility exists that the VDW interaction changes signs (that is, from repulsive to attractive) at very short separations. However, since no data are available on the Hamaker constant for the surface-active impurities, it is difficult to implement this mechanism to quantitatively examine how the absorbed layer affects bubble attachment in the impinging-jet experiment.

Furthermore, another possible reason for interception and attachment of bubbles, despite generally repulsive EDL and VDW interaction forces between gas bubbles and the collector surfaces, can be the presence of nanobubbles, recently demonstrated by Ishida et al. (2000) and Sakamoto et al. (2002) using the atomic-force microscopy technique (AFM). In their experiments, under normal conditions, long-range attractive forces are observed due to the presence of nanobubbles at hydrophobic surfaces. In another experiment reported by Ducker et al. (1994), strong long-range attraction forces were measured between a gas bubble and a hydrophilic silica particle and a hydrophobic silica plate. According to the experimental evidence, we can argue that any nanobubbles at the hydrophobic surface can coalesce, with gas bubbles approaching the collector surface as in our experiment, resulting in a positive Hamaker constant similar to an air–water–air system.

The hypothesis of heterogeneity of surface charges was twofold. One is the nonuniform discrete charge density (Kostoglou and Karabelas, 1992); the other is the fluctuation of the zeta potential (Prieve and Lin, 1982). Surface roughness is another type of surface inhomogeneity. In the literature, comprehensive reviews of the surface heterogeneity effects on particle deposition were furnished by Czarnecki (1986) and Walz (1998). Theoretical analyses showed that the whole interaction energy barrier could be greatly lowered with consideration of the surface heterogeneity effects, and possible local net attractive energy minima could occur for a case where a net repulsion was predicted for smooth surfaces. Consequently, particle deposition could occur at these local attractive minima. Using total internal reflection microscopy, the effect of surface roughness on colloidal interactions between a particle and a flat plate was shown experimentally by Lakkapragara and Walz (1997). They found the interaction energy barrier to be greatly lowered due to the presence of a rough surface. In the present experimental system, smooth gas bubbles interact with a relatively rough collector. The surface roughness image of the untreated glass scanned by the AFM technique is shown in Figure 12. The surface has a roughness (peak-to-valley) in the range of 10 to 30 nm, which is small compared to the bubble size but large compared to the EDL interaction thickness (the Debye–Hückel length is about 3 nm in 0.01 M NaCl) and the extent of the VDW interaction. The bubble is likely to experience fluctuations in local interaction energies as it travels along the collector surface. Accordingly, the effect of such surface roughness could substantially reduce the repulsive interaction energy.

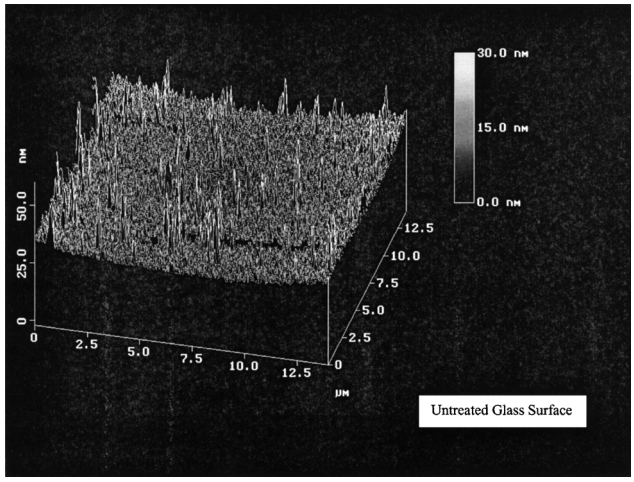

Figure 12. Surface roughness image of the untreated glass scanned by Atomic Force Microscope.

In addition, since the Boltzmann distribution is used to solve for the electric potential profile, the EDL interaction model presented here is valid only within the framework of equilibrium thermodynamics. Strictly speaking, this is not the case for bubble attachment where the colloidal interactions are essentially dynamic in nature. Thus, the interaction between a charged moving sphere and a charged stationary flat plate in a hydrodynamic flow becomes a complex coupled problem governed simultaneously by the Poisson equation, the general convective diffusion equation, and the equation of motion. As a result, the EDL interaction has to be reformulated to account for the combined hydrodynamic and electrokinetic interactions. The effect of hydrodynamic flow on the EDL interaction can be characterized using the Peclet number, which physically represents the relative importance of convection and diffusion and is defined as $Pe_i = u\kappa^{-1}/D$, where u is the ion velocity, κ^{-1} is the EDL thickness (taken as 10 nm), and D is the ion diffusion coefficient. In the im-

pinging-jet system, the appropriate ion velocity is of the order of $\alpha(\kappa^{-1})^2$. Assuming $\alpha = 1.0\times10^{6}\ \mathrm{s^{-1}\cdot m^{-1}}$(Yang, 2000) and $D = 1.0\times10^{-10}\mathrm{m^2\cdot s^{-1}}$, Pe is estimated to be of the order 10^{-8}. This suggests that, in the present situation, the perturbation of the Boltzmann distribution due to the presence of hydrodynamic flow is so small that the hydrodynamic convection effect on the EDL interaction can be neglected. Another recognized phenomenon related to the dynamic EDL effect is the electroviscous effect, which can be described as a change in the hydrodynamic interactions between a bubble and a collector due to the presence of electrostatic charges on the bubble and the collector surfaces. More specifically, $f_1(z)$, $f_2(z)$, $f_3(z)$, and $f_4(z)$ require modification. This electroviscous effect was examined by Warszynski and van de Ven (1991), who claimed that it could play an important role in particle coagulation and deposition. Analysis by Warszynski (2000) showed that particle mobility in the vicinity of the wall is a complex function of particle size, Debye length, and zeta potential. Only the electroviscous correction to $f_1(z)$ was provided. No modifications for $f_2(z)$, $f_3(z)$, and $f_4(z)$ are available. Nevertheless, for gas bubbles where κa_b is very large (at least several hundred), it is believed that the electroviscous effect is not significant (Warszynski and van de Ven, 1991).

In summary, based on the arguments just presented and the experimental conditions in this study, the observation that bubbles attach to hydrophilic untreated glass surfaces can be understood as follows: when bubbles are at great distances from the collector surface, the transport of bubbles is controlled by hydrodynamic and gravitational forces acting on the bubble. As the separation distance decreases to the order of a bubble radius, the hydrodynamic interaction between the bubble and the collector surface becomes appreciable. Since the hydrodynamic and gravity forces are dominant, they facilitate overcoming the resistance due to the colloidal repulsive interactions such that the bubbles can approach the collector surface to a distance of the order of several nanometers. Within this distance, the stability of the thin film, controlled by colloidal interactions between the bubble and the collector surface, plays a crucial role in bubble attachment. As discussed earlier, the existence of the aforementioned effects not only could lower the repulsive energy and create local net attractive energy minima, but may even result in rupture of the thin film. Consequently, bubble attachment would be achieved.

Clearly, the same arguments can also be applied to the attachment of bubbles to methylated glass and to explain the discrepancy between theory and experiment.

Bubble Attachment to Untreated and Methylated Glass Collectors

The videotape recording of the attachment process for untreated and methylated glass surfaces was reviewed to examine bubble behavior in the proximity of the collector at low Reynolds numbers. It was observed that the attachment characteristics for the untreated glass are considerably different from those for methylated glass. When the gas bubbles approached the untreated glass collector, they did not appear to instantaneously "stick" to the surface. Many bubbles rolled or slipped for short distances along the collector surface before they became attached, and most of the sliding bubbles were never immobilized. Bubbles attached to the untreated glass appeared to "stick" to the collector surface through a

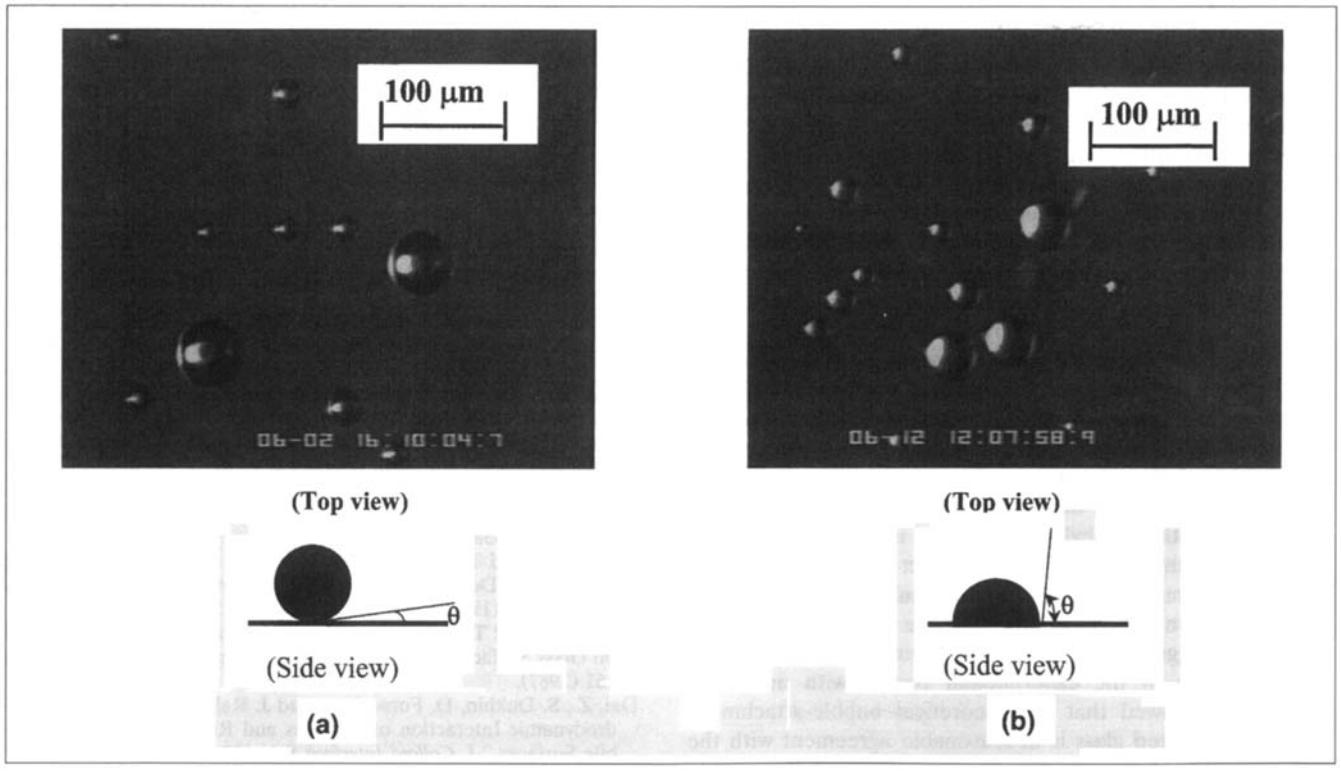

Figure 13. Microbubble attachment configuration on (a) untreated and (b) methylated glass surfaces.

small contact area, indicating small contact angles between the bubbles and the untreated glass (Figure 13a). Two types of attachment configurations are hypothesized here: one is similar to that for the methylated glass, where bubble attachment is the result of formation of a three-phase contact line; the other involves attachment due to local deformation of the bubble, essentially the same mechanism as solid-particle deposition. Therefore, for the latter situation, the formation of a three-phase contact line may not be necessary for bubble attachment.

In contrast, for the methylated glass experiments, there were nearly no instances of bubble detachment. Once a bubble collided with the methylated glass collector, the bubble appeared to adhere strongly to the collector, even at fairly high Reynolds numbers. This implies that more force is needed to detach attached bubbles from the methylated glass than from the untreated glass. Bubble attachment onto a hydrophobic surface is related to drainage of the thin liquid film between the bubble and the collector surface. If such a thin film becomes unstable or is broken, a three-phase contact line is created and a contact angle is formed. It was observed that when bubbles landed on the methylated glass, the thin liquid film between the bubble and the methylated glass was ruptured instantly. This suggests that "induction time" is very short under such conditions. As shown in Figure 13b, the diameter of the contact area between the attached bubble and the methylated glass surface is nearly the same as the bubble size, thus indicating a relatively large contact angle, close to 90°. Attached bubbles can be immobilized by both contact-angle hysteresis and surface force at the three-phase contact line.

Summary

The impinging-jet technique provides an effective means for studying bubble–solid surface interaction and attachment under well-controlled hydrodynamic conditions. Two types of collectors, namely, methylated and untreated glass surfaces, were used in this work. The contact angles for the methylated and untreated glass surfaces are about 90° and less than 10°, respectively. The process of bubble attachment onto a solid surface was not only found to be significantly affected by the hydrodynamic conditions, but is also noticeably dependent on the EDL parameters. Experimental results showed that for a given set of fixed physicochemical conditions, the normalized bubble-attachment density increases with increasing Reynolds number within the range of Re studied. Furthermore, the number of attached bubbles was found to vary linearly with time, indicating negligible blocking effects during the period of an experimental run. In addition, bubble-attachment experiments demonstrated that the bubble-attachment flux to the methylated collector is much higher than that to the untreated collector. Direct observation of the bubble-attachment process revealed substantially different behaviors when bubbles approached the vicinity of these two collectors, suggesting different attachment mechanisms.

Comparison of the experimental results with numerical predictions showed that the theoretical bubble-attachment flux to methylated glass is in reasonable agreement with the experimental values, attesting to the validity of the bubble transport model developed on the basis of the DLVO theory. It was found that the theoretically predicted attachment flux to untreated glass matches well with experimentally measured values only when the Reynolds number is high ($Re \geq 400$); the proposed model failed to predict bubble attachment onto the untreated glass surface at Reynolds numbers in the range of $100 \leq Re \leq 300$. It was also noted that, since both the VDW interaction of the bubble–water–glass system and the EDL interaction between the bubble and the untreated glass are repulsive, the evidence of bubble attachment onto untreated (hydrophilic) glass surfaces could not be explained on the basis of existing thin-film theories. Consequently, several mechanisms including absorbed surface-active impurity layer and stochastic effects were postulated to account for bubble attachment onto glass surfaces. However, it seems that further investigation is needed to identify the dominating factors and draw firm conclusions.

Acknowledgments

Financial support from the Natural Sciences and Engineering Research Council of Canada (NSERC Industrial Research Chair in Oil Sands Engineering) to Jacob Masliyah and the Andrew Stewart Memorial Graduate Scholarship from the University of Alberta to C. Yang are acknowledged. The authors are also grateful for support and assistance of the personnel at Syncrude Canada Ltd., Edmonton Research Centre.

Literature Cited

Acrivos, A., and T. D. Taylor, "Heat and Mass Transfer from Single Spheres in Stokes Flow," *Phys. Fluids*, **5**, 387 (1962).

Adamczyk, Z., T. Dabros, J. Czarnecki, and T. G. M. van de Ven, "Particle Transfer to Solid Surfaces," *Adv. Colloid Interface Sci.*, **19**, 183 (1983).

Anderson, J. L., "Colloidal Transport by Interfacial Forces," *Ann. Rev. Fluid Mech.*, **21**, 61 (1989).

Araujo, Y. C., P. G. Toledo, V. Leon, and H. Y. Gonzalez, "Wettability of Silane-Treated Glass Slides as Determined from X-Ray Photoelectron Spectroscopy," *J. Colloid Interface Sci.*, **176,** 485 (1995).

Bohmer, M. R., E. A. van der Zeeuw, and G. J. M. Koper, "Kinetics of Particle Adsorption in Stagnation Point Flow Studied by Optical Reflectometry," *J. Colloid Interface Sci.*, **197**, 242 (1998).

Burn, S. E., S. Yiacoumi, and C. Tsouris, "Microbubble Generation for Environmental and Industrial Separation," *Sep. Purif. Technol.*, **11**, 221 (1997).

Czarnecki, J., and T. Dabros, "Attenuation of the van der Waals Attraction Energy in Particle/Semi-Infinite Medium System Due to the Roughness of Particle Surface," *J. Colloid Interface Sci.*, **78**, 25 (1980).

Czarnecki, J., "van der Waals Attraction Energy Between Unequal Rough Spherical Particles," *J. Colloid Interface Sci.*, **98**, 590 (1984).

Czarnecki, J., "The Effects of Surface Inhomogeneities on the Interreactions in Colloidal Systems and Colloid Stability," *Adv. Colloid Interface Sci.*, **24**, 283 (1986).

Dabros, T., and T. G. M. van de Ven, "Kinetics of Coating by Colloidal Particles," *J. Colloid Interface Sci.*, **89**, 232 (1982).

Dabros, T., and T. G. M. van de Ven, "A Direct Method for Studying Particle Deposition onto Solid Surfaces," *Colloid Polym. Sci.*, **261**, 694 (1983a).

Dabros, T., and T. G. M. van de Ven, "On the Effects of Blocking and Particle Detachment on Coating Kinetics," *J. Colloid Interface Sci.*, **93**, 576 (1983b).

Dabros, T., and T. G. M. van de Ven, "Deposition of Latex Particles on Glass Surfaces in an Impinging Jet," *Physicochem. Hydrodyn.*, **8**, 161 (1987).

Dai, Z., S. Dukhin, D. Fornasiero, and J. Ralston, "The Inertial Hydrodynamic Interaction of Particles and Rising Bubbles with Mobile Surfaces," *J. Colloid Interface Sci.*, **197**, 275 (1998).

Deshpande, M. D., and R. N. Vaishnav, "Submerged Laminar Jet Impingement on a Plane," *J. Fluid Mech.*, **114**, 213 (1982).

Dijt, J. C., M. A. Stuwart, J. E. Hofman, and G. J. Fleer, "Kinetics of Polymer Adsorption in Stagnation Point Flow," *Colloids Surf. A*, **51**, 141 (1990).
Ducker, W. A., Z. Xu, and J. N. Israelachvili, "Measurements of Hydrophobic and DLVO Forces in Bubble-Surface Interactions in Aqueous Solutions," *Langmuir*, **10**, 3279 (1994).
Elimelech, M., and C. R. O'Melia, "Effect of Particle Size on Collision Efficiency in the Deposition of Brownian Particles with Electrostatic Energy Barriers," *Langmuir,* **6**, 1153 (1990).
Elimelech, M., "Kinetics of Capture of Colloidal Particles in Packed Beds under Attractive Double Layer Interactions," *J. Colloid Interface Sci.*, **146**, 337 (1991).
Fukui, Y., and S. Yuu, "Collection of Submicron Particles in Electro-Flotation," *Chem. Eng. Sci.*, **35**, 1097 (1980).
Goldman, A. J., R. G. Cox, and H. Brenner, "Slow Viscous Motion of a Sphere Parallel to a Plane Wall," *Chem. Eng. Sci.*, **22**, 653 (1967).
Goren, S. L., and M. E. O'Neill, "On the Hydrodynamic Resistance to a Particle of a Dilute Suspension when in the Neighbourhood of a Large Obstacle," *Chem. Eng. Sci.*, **26**, 325 (1971).
Hogg, R., T. W. Healy, and D. W. Fuerstenau, "Mutual Coagulation of Colloidal Dispersions," *Trans. Faraday Soc.*, **62**, 1638 (1966).
Hunter, R. J., *Zeta Potentials in Colloid Science: Principles and Applications*, Academic Press, New York (1981).
Ishida, N., M. Sakamoto, M. Miyahara, and K. Higashitani, "Attraction between Hydrophobic Surfaces with and Without Gas Phase," *Langmuir*, **16**, 5681 (2000).
Israelachvili, J. N., *Intermolecular and Surface Forces*, 2nd ed., Academic Press, London (1985).
Kim, S., and S. J. Karrila, *Microhydrodynamics: Principles and Selected Application*, Butterworth-Heinemann, Boston (1991).
Kostoglou, M., and A. J. Karabelsas, "The Effect of Discrete Surface Charge on Potential Energy of Repulsion Between Colloidal Surfaces," *J. Colloid Interface Sci.*, **151**, 534 (1992).
Lakkapragara, S., and J. Y. Walz, "Direct Measurement of the Effect of Surface Roughness on the Colloidal Forces between a Particle and Flat Plate," *J. Colloid Interface Sci.*, **196**, 177 (1997).
Larsen, A. E., and D. G. Grier, "Like-Charge Attraction in Metastable Colloidal Crystallites," *Nature*, **385**, 230 (1997).
Leppinen, D. M., "Trajectory Analysis and Collision Efficiency During Microbubble Flotation," *J. Colloid Interface Sci.*, **212**, 431 (1999).
Loewenberg, M., and R. H. Davis, "Flotation Rates of Fine, Spherical Particles and Droplets," *Chem. Eng. Sci.*, **49**, 3923 (1994).
Luttrell, G. H., and R. H. Yoon, "A Hydrodynamic Model for Bubble–Particle Attachment," *J. Colloid Interface Sci.,* **154,** 129 (1992).
Masliyah, J. H., *Electrokinetic Transport Phenomena,* Alberta Oil Sands Technol. and Res. Authority Tech. Pub. Ser. No. 12, Edmonton, Alta., Canada (1994).
McCormack, D., S. Carnie, and D. Y. C. Chan, "Calculations of Electric Double-Layer Force and Interaction Free Energy Between Dissimilar Surfaces," *J. Colloid Interface Sci.*, **169**, 177 (1995).
Prieve, D. C., and E. Ruckenstein, "Effect of London Forces upon the Rate of Deposition of Brownian Particles," *AIChE J.,* **20**, 1178 (1974).
Prieve, D. C., and M. M. J. Lin, "The Effect of Distribution in Surface Properties on Colloid Stability," *J. Colloid Interface Sci.*, **86**, 17 (1982).
Ramirez, J. A., A. Zinchenko, M. Loewenberg, and R. H. Davis, "The Flotation Rates of Fine Spherical Particles Under Brownian and Convection Motion," *Chem. Eng. Sci.,* **54**, 149 (1999).
Sakamoto, M., Y. Kanda, M. Miyahara, and K. Higashitani, "Origin of Long Range Attractive Force Between Surfaces Hydrophobized by Surfactant Adsorption," *Langmuir*, **18**, 5713 (2002).
Sanders, R. S., R. S. Chow, and J. H. Masliyah, "Deposition of Bitumen and Asphaltene-Stabilized Emulsions in an Impinging Jet Cell," *J. Colloid Interface Sci.,* **174**, 230 (1995).
Sharma, A., and A. Jameel, "Nonlinear Stability, Rupture, and Morphological Phase Separation of Thin Fluid Films on Apolar and Polar Substrates," *J. Colloid Interface Sci.,* **161**, 190 (1993).
Suzuki, A., N. F. H. Ho, and W. I. Higuchi, "Prediction of the Particle Size Distribution Changes in Emulsions and Suspensions by Digital Computation," *J. Colloid Interface Sci.*, **29**, 552 (1969).
Usui, S., and E. Barouch, "Effect of Adsorbed Layers on the van der Waals Interaction between Particles and Bubbles in Aqueous Media," *J. Colloid Interface Sci.,* **137,** 281 (1990).
van de Ven, T. G. M., *Colloidal Hydrodynamics*, Academic Press, San Diego, CA (1989).
Varennes, S., and T. G. M. van de Ven, "Deposition and Detachment of Latex Particles at Glass Surfaces Exposed to Flow," *Physicochem. Hydrodyn.*, **9**, 537 (1987).
Vincent, B., "The van der Waals Attraction Between Colloid Particles Having Adsorbed Layers: II. Calculation of Interaction Curves," *J. Colloid Interface Sci.*, **42**, 270 (1973).
Vinke, H., P. J. Hamersma, and J. M. H. Fortuin, "Particle-to-Bubble Adhesion in Gas/Liquid/Solid Slurries," *AIChE J.*, **37**, 1801 (1991).
Walz, J. Y., "The Effect of Surface Heterogeneities on Colloidal Forces," *Adv. Colloid Interface Sci.*, **74**, 119 (1998).
Warszynski, P., and T. G. M. van de Ven, "Effect of Electroviscous Drag on the Coagulation and Deposition of Electrically Charged Colloidal Particles," *Adv. Colloid Interface Sci.*, **36**, 33 (1991).
Warszynski, P., "Coupling of Hydrodynamic and Electric Interactions in Adsorption of Colloidal Particles," *Adv. Colloid Interface Sci.*, **84**, 47 (2000).
Yang, C., T. Dabros, D. Li, J. Czarnecki, and J. H. Masliyah, "An Analysis of Fine Bubbles Attachment onto a Solid Surface Within the Framework of DLVO Theory," *J. Colloid Interface Sci.*, **219**, 69 (1999).
Yang, C., "Attachment of Fine Bubbles onto a Solid Surface and Electrokinetics of Gas Bubbles," PhD Diss., Univ. of Alberta, Edmonton, Alta., Canada (2000).
Yang, C., T. Dabros, D. Li, J. Czarnecki, and J. H. Masliyah, "Measurement of the Zeta Potential of Gas Bubbles in Aqueous Solutions by Microelectrophoresis Method," *J. Colloid Interface Sci.*, **243**, 128 (2001).

Manuscript received Jan. 3, 2002, and revision received Oct. 15, 2002.